Applied Physics A (2019) 125:489
https://doi.org/10.1007/s00339-019-2785-4

Applied Physics A
Materials Science & Processing

Synthesis and evaluation of the structural, optical, and antibacterial properties of copper oxide nanoparticles

Suresh Sagadevan[1] · S. Vennila[2] · A. R. Marlinda[1] · Yarub Al-Douri[1] · Mohd. Rafie Johan[1] · J. Anita Lett[3]

Received: 12 April 2019 / Accepted: 3 July 2019 / Published online: 5 July 2019

Abstract
The nanostructured material, due to their outstanding applications in various fields of science and technology; metal and metal oxide nano are exclusively explored in the progress of nanosized materials. The transition metal oxides including CuO is are used for magnetic storage devices, solar energy applications, sensors, as a catalyst in reactions, as electrode materials in supercapacitors and to tune the semiconducting properties of materials. The current work focuses on the synthesis of CuO nanoparticles (NPs) by combustion technique for various annealing (100°C and 300°C) using ascorbic acid as a capping agent. The XRD pattern confirms that the CuO NPs exhibit the monoclinic structure. The optical properties are investigated using UV–Vis absorption spectra. Further, the refractive index, optical dielectric constant and bulk modulus were investigated using the specific empirical model as a function of temperature. The FTIR spectrum shows that the band in the range 450–500 cm^{-1} confirms the formation of CuO NPs. The SEM images revealed that the spherical surface morphology of the CuO NPs. The Elemental analysis and the particle size were confirmed by elemental dispersive X-ray analysis (EDX) and particle size analyzer. Moreover, the antibacterial activity of CuO nanoparticles was investigated using *E. coli*, *S. typhi*, *M. luteus*, *P. fluorescent*, *S. flexneri*, and *V. cholera* bacteria.

1 Introduction

Nanotechnology is seen as the development of the next generation of technology with applications in many fields through which existing materials, virtually all man-made materials, and systems, can acquire various properties making them suitable for new applications. In recent years, synthesis processes to grow dispersed nanoparticles in a matrix have attracted the attention of several researchers. However, the growth of dispersed nanoparticles with homogenous sizes is not easy. Nanoparticles of metal oxide are an important class of semiconductors that have applications in storage media, electronics, solar power, and catalysis [1–4]. Because of its unique physical and chemical properties, CuO NPs has attracted considerable attention as catalyst materials, solar cells, optoelectronic devices, antibacterial materials, lithium batteries, and so on [5–8]. Due to their distinctive physical–chemical properties, research interest in nanoparticles has improved rapidly. In terms of diffusivity, electrical resistivity, and electrical conducting property, nanomaterials are completely different from bulk materials. The strength of nanomaterials and nanomaterial chemical reactivities differ from that of bulk materials [9–11]. Because of their thermostability with different functionalities, metal or metal oxide nanoparticles such as Ag, ZnO, and CuO nanoparticles attract attention as useful nanomaterials [12]. Copper oxide nanoparticles (CuO NPs) of these nanomaterials have attracted considerable attention due to the low cost of production, thermal stability, relatively low toxicity, and strong antibacterial activity [13–17]. Cuprous and cupric oxides (Cu_2O and CuO) are gaining more attention as promising materials for optoelectronic applications due to the low environmental toxicity and abundance in the earth's crust [18–24]. In the range 2.0–2.5 eV and 1.3–1.7 eV both Cu_2O and CuO are direct bandgap semiconductors [25, 26]. Depending on the conditions of growth, their absorption spectrum covers a large part of the UV vs NIR region. Based on Shockley and Queisser's thermodynamic consideration, CuO's bandgap (almost 1.45 eV) is best suited for achieving

✉ Suresh Sagadevan
drsureshnano@gmail.com

[1] Nanotechnology and Catalysis Research Centre, University of Malaya, 50603 Kuala Lumpur, Malaysia

[2] PG Research Department of Physics, Jayaraj Annapackiyam College For Women (Autonomous), Periyakulam, Tamilnadu 625 605, India

[3] Department of Physics, Sathyabama Institute of Science and Technology, Chennai 600 119, India

the highest efficiency [27, 28]. Very few works have focused on the effect of annealing temperature in the synthesis of CuO by combustion technique. Hence, the main objective of this work is to investigate the effect of annealing temperature of the starting precursors using ascorbic acid as a capping agent on the structural properties of CuO nanostructures synthesized through the method of combustion. Additionally, the optical, morphological and antibacterial properties were also analyzed.

2 Methods and materials

2.1 Chemicals

All chemicals used in the experiment including copper acetate pentahydrate and ascorbic acid were analytical grade reagents and were used with no further refinement. Throughout the experiment, double distilled water was used.

2.2 CuO nanoparticles preparation

For the synthesis of CuO NPs, typical 1 mM aqueous solution of copper acetate pentahydrate was prepared in a conical flask, to which ascorbic acid was added by dropwise addition method with continuous stirring at the rate of 500 rpm. The composition of the solution components, (fuel and oxidizer) was calculated according to the principle of propellant chemistry. The temperature of the reaction was increased from 100 °C to 300 °C by constant stirring. At this temperature, the solution reaches the point of combustion. Hence, the solution starts burning to release a lot of heat as fumes and vaporizing the whole solution. Within a period of 15 min, the whole combustion reaction was completed leaving behind fine black colored nanopowder followed by a large amount of black precipitate. These precipitates were then centrifuged and washed several times with deionized water. Finally, these collected black precipitates were air dried for a time period of 2 h. The schematic representation of the synthesis CuO NPs is shown in Fig. 1. The samples were sintered at two different temperatures, 100 °C and 300 °C and were further used for characterization.

2.3 Antibacterial activity

Antimicrobial activity of CuO NPs was carried out by standard agar disk diffusion method against bacterial strains (*E. coli* and *S. Typhi*), Gram-positive bacterium (*M. luteus*) and Gram-negative bacterium (*S. flexneri*, *P. fluorescent*, *V. cholera* bacteria). Nutrient ager (1 g beef extract, 1 g peptone, 0.5 g NaCl dissolved in 100 ml of double distilled water) was used to cultivate bacteria. The growth media was autoclaved and cooled normally. The media was then poured into the Petri dishes and kept for 30 min for solidification. After 30 min the fresh overnight cultures of inoculums (100 µl) of different culture were swabbed over the agar plates using a sterile cotton swab. The sterile disk (5 mm) was impregnated with 100 µg ml^{-1} of CuO NPs (uniform concentration) and was placed over the bacterial lawns. The antibiotic, erythromycin loaded sterile disk acted as a control and the plates were incubated at 37 °C for 24 h. The plates were then incubated in the incubator at 37 °C for 24 h and then they were observed visually for the formation of a zone of inhibition (ZOI) measured as diameter (mm). All the studies were conducted in triplicates.

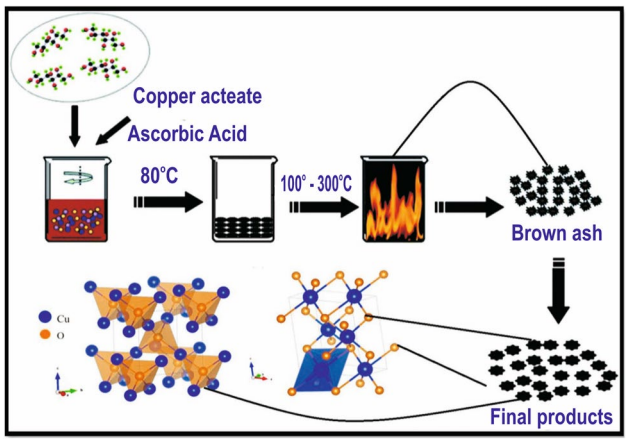

Fig. 1 The schematic diagram representation of the synthesis CuO NPs

2.4 Characterization technique

X-ray diffraction was conducted on a Philips Analytical XPERT diffractometer using a Cu Kα radiation ($\lambda = 1.54056$ A°) with a MINIPROP detector and operating at 40 kV and 40 mA. The identification of functional groups was done using an FTIR spectrophotometer (JASCO FT-IR 4700). The surface morphology of the prepared CuO NPs was examined by scanning electron microscope (SEM) using PHILIP XL-30 and elemental analysis was investigated by electron dispersive X-ray (EDX) attached to SEM. UV–visible spectra of the CuO NPs were analyzed by a Hitachi (U-2001, Tokyo, Japan) UV-spectrophotometer.

3 Results and discussion

3.1 X-ray diffraction analysis

XRD has been a rapid analytical technique used primarily to identify the phase of a crystalline material and deliver information on lattice parameters. The XRD pattern of CuO NPs sintered at 100 °C and 300 °C are shown in Fig. 2. The XRD

peak positions were consistent with CuO and sharp peaks with a high intensity of XRD indicate the crystalline nature. XRD peaks confirm that CuO was formed in a monoclinic structure and the lattice parameters of the unit cells are $a = 4.683$ Å, $b = 3.421$ Å, $c = 5.129$ Å, having $\beta = 99.252$ Å. The observed diffraction patterns correspond to the crystal planes of CuO (110), (002), (200) and (202), respectively. The observed diffraction patterns are well matched with the reported literature and JCPDS 80-1268. Except for CuO, no other diffraction peaks are observed in the pattern which confirmed that the synthesized materials are pure CuO without any significant impurity. In addition, all the peaks are sharp and strong which revealed the well-crystallinity of the synthesized CuO nanostructures. The increase in intensity peak was obtained after calcination and the XRD pattern is still identical to the precipitate pattern as prepared. This result indicates that enough nucleation energy from thermal treatment has enhanced CuO's crystallinity. The basic crystal of as-synthesized CuO appeared indistinctly for copper acetate material, but the presence of CuO peaks was stronger following the process of calculations. CuO receives good crystallinity of CuO compared to different temperatures and increases in crystallinity and its size after annealing treatment can be effectively achieved. The average crystallite size of the CuO NPs was calculated using the Debye–Scherrer equation:

$$D = \mathrm{K}\,\lambda/\beta\cos\theta, \tag{1}$$

Where D is the crystallite size (nm), λ represents wavelength of X-ray source (0.15406 A°), β is the full width at half maximum of the diffraction peak (FWHM) in radians, K is the Scherrer constant with value from 0.9 to 1, θ is the Bragg angle

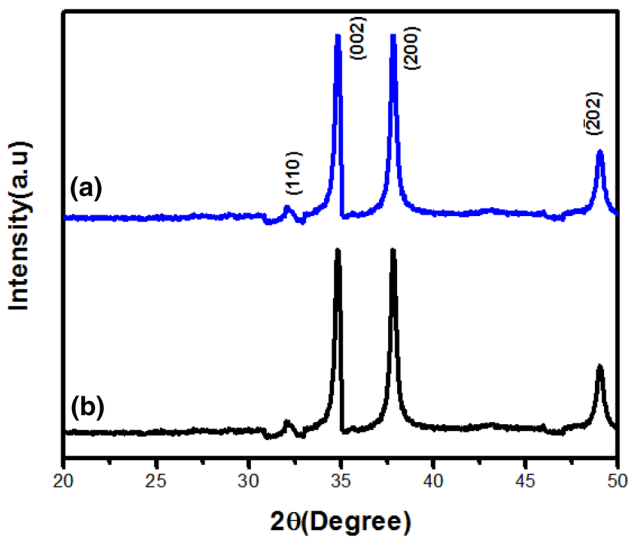

Fig. 2 The XRD pattern of CuO NPs **a** 100°C and **b** 300°C, respectively

in (degree). The average crystallite size found to be about 45 and 36 nm for 100°C and 300°C, respectively. Thus, the annealing temperature plays an important role in reducing the size of the nanoparticles; higher the annealing temperature used for the synthesis, smaller is the nanoparticles obtained by combustion method using ascorbic acid as a capping agent.

The three empirical models employed to calculate the refractive index using energy gap values were described in the present study. It is a measure of how light propagates through a material. The refractive index can provide information about light behavior. When light passes through the materials, its velocity decreases by increasing the material refractive index. An important physical parameter in microscopic atomic interactions is the refractive index *(n)*. In theory, the refracting index is associated with these entities' density and local polarizability [29]. There were attempts to investigate many simple relationships between the energy gap (E_g) and refractive index (n) [30]. To validate the current work, various links between E_g and n have been reviewed. A linear relationship presenting high-frequency refractive index and the band gap is suggested by Ravindra et al. [30]:

$$n = \alpha + \beta E_{\mathrm{g}}, \tag{2}$$

where $\alpha = 4.048$ and $\beta = -0.62$ eV^{-1}. Taking inspirations from the simple physics of light dispersion and refraction, the following empirical relation was proposed by Herve and Vandamme [31]:

$$n = \sqrt{1 + \left(\frac{A}{E_{\mathrm{g}} + B}\right)^2} \tag{3}$$

in which $A = 13.6$ eV and $B = 3.4$ eV.

A distinct method was taken by Ghosh et al. [32], to consider the concept of Penn [33] and Van Vechten [34] for quantum–dielectric formulations and band structure. A is a contribution from the valence electrons and B is a constant added to the lowest band gap E_g, the following expression was developed:

$$n^2 - 1 = A/\left(E_{\mathrm{g}} + B\right)^2. \tag{4}$$

In which $A = 25E_g + 212$, $B = 0.21E_g + 4.25$ and $(E_g + B)$ refers to a suitable average energy space of material. As such, there were attempts by these three models for variation of n with an energy gap. Furthermore, the equation $\varepsilon_\infty = n^2$ was utilized to calculate the optical dielectric constant (ε_∞) [35]. Table 1 lists the investigated refractive index and optical dielectric constant at different temperatures. It proves that the Ghosh et al. model is a suitable one for the application. Lattice constant may be linked to bulk modulus, with major influence being the covalency degree characterized by Phillips' homopolar gap E_h [36]. A stimulus to present this information is the verification of

our calculation that is non-restricted to computed space. As such, we trust that this data will be useful for future investigations. The clear distinction between lattice constants for CuO nanoparticles, as observed in Table 1, provides an incentive to investigate B_0 at different temperatures. The lattice constant as observed in Table 1 is the basis of our model. The following empirical formula is provided by the fitting of these data [37]:

$$B_0 = [3000 - 100\lambda]\left(\frac{a}{2}\right)^{-3.5}. \quad (5)$$

In which a (in Å), the lattice constant, while the empirical parameter which accounts for the influence of iconicity is represented by λ: with $\lambda = 0, 1, 2$, respectively. The temperature effect causes the CuO nanoparticles bulk modulus to have a specific value.

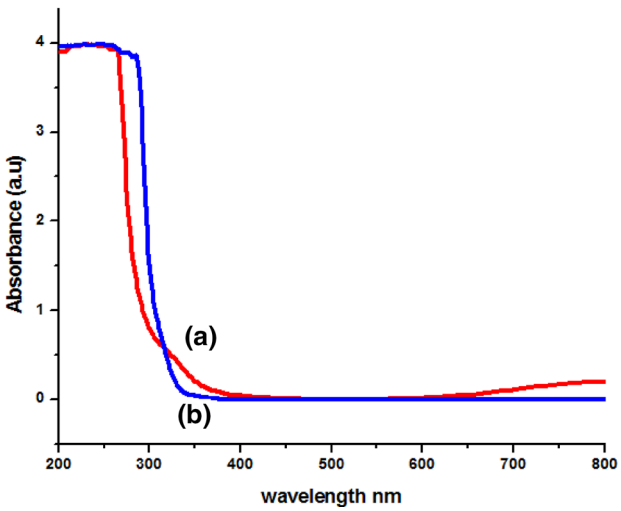

Fig. 3 UV–Vis analysis of CuO NPs for **a** 100°C and **b** 300°C, respectively

3.2 UV–Vis Spectroscopy analysis

UV–Vis spectrum, shown in Fig. 3a, b, studied the optical properties of CuO NPs for 100°C and 300 °C, respectively. The lower shift in wavelength or blue shift is attributed to the effect of Burstein–Moss, which confirms the effect of quantum containment [38]. In the UV-region, the absorption peaks appeared at wavelengths of approximately 266 nm and 269 nm for 100 °C and 300 °C, respectively. The edge of absorption is observed in the 240–270 nm range. This blue shift of the absorption edges for various sizes of nanocrystals is related to particle size reduction because of nanoparticles on quantum containment. CuO nanoparticles lower band bap value exhibits the nature of the blue shift in the nanoscale region because of quantum containment [39].

3.3 Fourier transform infrared spectroscopy (FTIR) studies

Figure 4a, b showed the FTIR spectrum of CuO NPs for 100°C and 300°C, respectively. FTIR spectra were recorded in the range of 4000–500 cm^{-1}. The bands which are in the range of 3200–3800 cm^{-1} are attributed to O–H stretching vibration of water absorbed by the sample. The bands observed in the range of 2350–2360 cm^{-1} may be due to NH_3^+ stretching vibration. The bands observed in the range of 1700–1710 cm^{-1} may be due to C = O stretching vibration. The band observed around 1500 cm^{-1} may be due to N–O asymmetric stretching. The CuO nanoparticles displayed 432 cm^{-1}, 611 cm^{-1} vibration modes for Cu–O stretching vibration, 886 cm^{-1} rocking vibration mode of the water molecule and 1640 cm^{-1} and 3100–3500 cm^{-1} absorption bands. The vibration of the Cu–O stretch is assigned at 623 cm^{-1}. The 450–550 cm^{-1} bands confirmed CuO NP's presence [40].

3.4 SEM and EDAX analysis

The morphological and structural properties of the CuO nanoparticles were observed using SEM. The SEM images

Table 1 The energy gap, refractive index, and optical dielectric constant of CuO nanoparticles correspond to lattice constants and bulk modulus

Temperature (°C)	E_g (eV)	Refractive index (n)	Optical dielectric constant (ε_∞)	Lattice constants (Å)	Bulk modulus (B_0) (GPa)
100	4.670	1.152[a] 1.017[b] 2.080[c]	1.327[a] 1.034[b] 4.326[c]	$a = 4.683$ $b = 3.421$ $c = 5.129$	142.538
300	4.618	1.180[a] 1.017[b] 2.090[c]	1.392[a] 1.034[b] 4.368[c]	$a = 4.685$ $b = 3.423$ $c = 5.132$	142.537

[a]Ravindra et al. [30]

[b]Herve and Vandamme [31]

[c]Ghosh et al. [32]

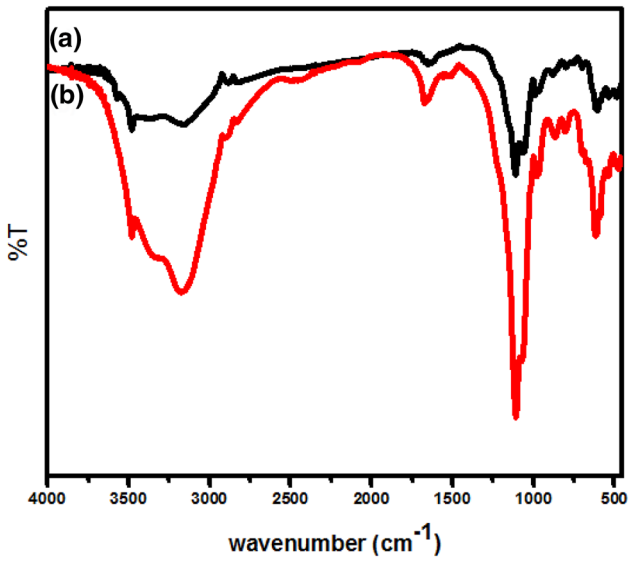

Fig. 4 The FTIR analysis of CuO NPs for **a** 100°C and **b** 300°C, respectively

of CuO NPs as shown in Fig. 5. The synthesized CuO NPs had sizes which are in the nanometer range and their structures were not homogenous. These images indicate that only a few nanoparticles with spherical shape were synthesized. Some nanoparticles were well separated from each other while most were present in the agglomerated form. Thus, these SEM results confirmed the nanostructure behavior of the synthesized particles. Further, the SEM micrograph revealed that the CuO NPs is porous and agglomerated. The pores and voids can be attributed to the amount of gases that escaped during combustion. The process of agglomeration takes place because of an increase in the rate of nucleation of the particles at a higher temperature. In the initial stage, the aqueous combination of Cu^{2+} and malic acid leads to the first nucleation seeds which act as an initial nucleus along with the growth of particles. The combustion process was gradually inherited from the high temperature and uniform size particles were obtained. Accordingly, the heat released in combustion changes and thus the enthalpy, which is responsible for the formation of different structures. At some places, the particles seemed to be agglomerated. The elemental quantification and stoichiometric ratio of CuO NPs were confirmed by energy-dispersive X-ray analysis (EDX), which showed the presence of a uniform distribution of copper to oxygen (atomic ration of 1:1) in CuO NPs as shown in Fig. 6.

3.5 Antibacterial activity

The antibacterial activity of CuO NPs was tested *E. coli, S. typhi, M. luteus, P. fluorescens, S. flexneri* and *V. cholerae*, and the results are shown in Fig. 7. Maximum inhibition zone was obtained against *M.luteus* (7 ± 0.22 mm) followed by *S. typhi* (5 ± 0.133 mm) and *E. coli* and *P. fluorescens*(3 ± 0.17 mm) by the CuO NPs. From the present study, it is inferred that the bacterial Gram-positive strains are less affected than Gram-negative bacterial strains. The variation in the sensitivity or resistance of population of both Gram-positive and negative bacteria may be due to differences in cell structure, physiology, metabolism or degree of contact with nanoparticles by organisms. Due to electrostatic forces, the opposite charges of bacteria and copper ions released from nanoparticles are believed to cause adhesion and bioactivity. Since peptidoglycans are negatively charged molecules, they bind Cu^{2+} ions released from copper NPs in the liquid growth medium. Being Gram-negative, the bacterium *E. coli* may allow more Cu^{2+} ions to reach the plasma membrane but is generally considered less susceptible to antibiotics and antibacterial agents than Gram-positive bacteria [41]. Finally, it can be concluded that because of their membrane structure, Gram-negative bacterial strains show higher antimicrobial activity than Gram-positive. Because of their opposite electrical charges resulting in a reduction at the bacterial cell wall, the antibacterial properties of copper NPs are primarily attributed to adhesion with bacteria. There are differences between Gram-positive and Gram-negative bacteria in their membrane structure, the most distinctive of which is peptidoglycan layer thickness. As a result, the bactericidal effects observed in this study may have been influenced by the solution release of Cu^{2+} ions. The binding of copper ions to the bacterial cell surface is believed to play an important role in bactericidal activity from these results.

The antimicrobial activity against various microorganisms (Gram-negative), *Klebsiella pneumonia*, *Acinetobacter baumannii*, *Pseudomonas aeruginosa*, *Citrobacter freundii*, *Escherichia coli*, *Vibrio cholerae* were evaluated in this study as shown in Fig. 8. Based on the inhibition zone, the antibacterial activity of CuO NPs was quantitatively evaluated. The CuO NPs are exhibiting effective bacterial resistance against Gram-negative bacteria. Goyal et al. also testified that the antimicrobial characteristics rest on the surface characteristics and the size of CuO nanoparticles. It appears that smaller particles intended through the large surface area have improved antibacterial activity, as associated with bigger CuO nanoparticles. CuO nanoparticles disclosed a chief antimicrobial activity against Bacillus subtilis [42]. El-Nahhal et al. enhanced the antibacterial activity of CuO nanoparticles with coated cotton bandages and CuS nanoparticle using cotton bandages. Surprisingly, the sample containing CuO nanoparticles exhibited larger antibacterial activity than others with no reduction in the viability of tested bacteria [43].

Additionally, comparatively we can conclude the CuO NPs exhibit effective bacterial resistance against

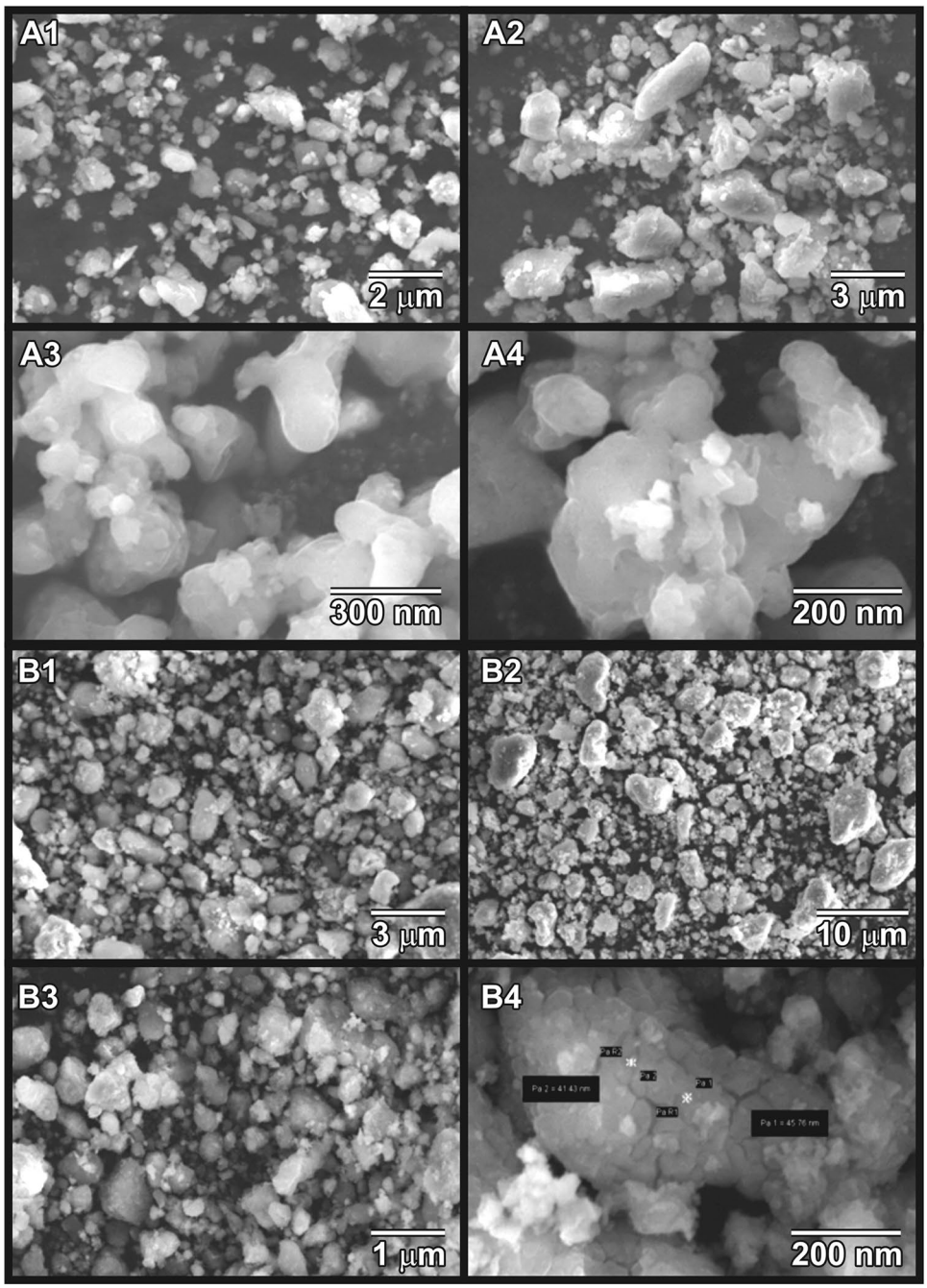

Fig. 5 SEM images for CuO NPs for **a1**–**a4** 100°C and **b1**–**b4** 300°C, respectively

Gram-negative bacteria. Although, CuO nanoparticles have great biological characteristics which embrace effective antimicrobial action against a wide range of Gram-positive and Gram-negative pathogens and also drug-resistant bacteria. These properties have directed to the growth of numerous approaches with unswerving applications to the biomedical field, such as custom-made surfaces through antimicrobial effect, wound dressings and improved textiles [44]. It is also believed that these nanosystems could represent efficient alternatives in the expansion of smart systems exploited for both recognition of pathogens and for the treatment of infections.

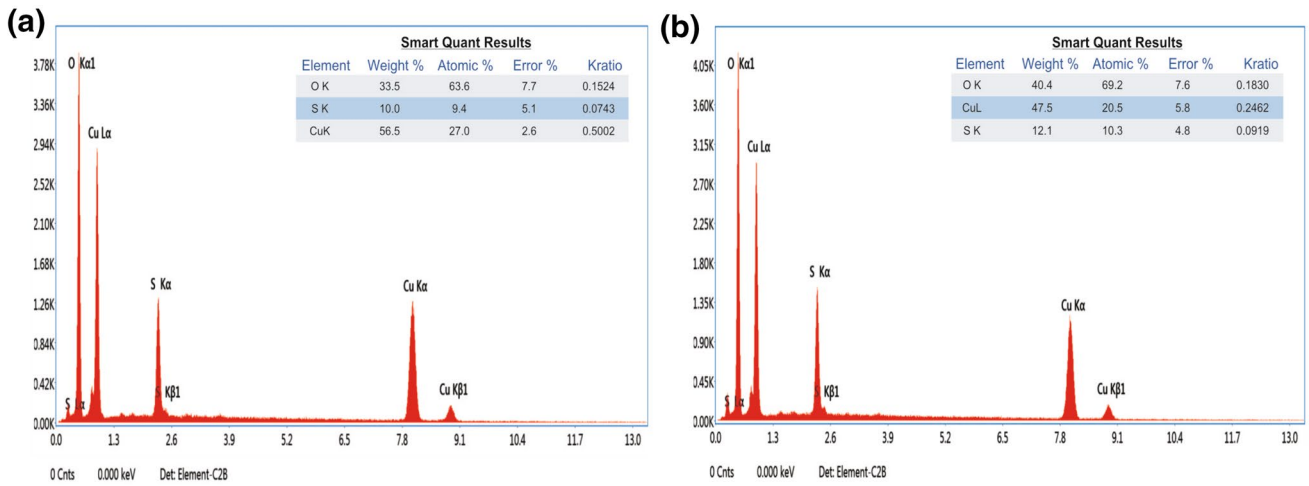

Fig. 6 EDAX analysis for CuO NPs for **a** 100°C and **b** 300°C, respectively

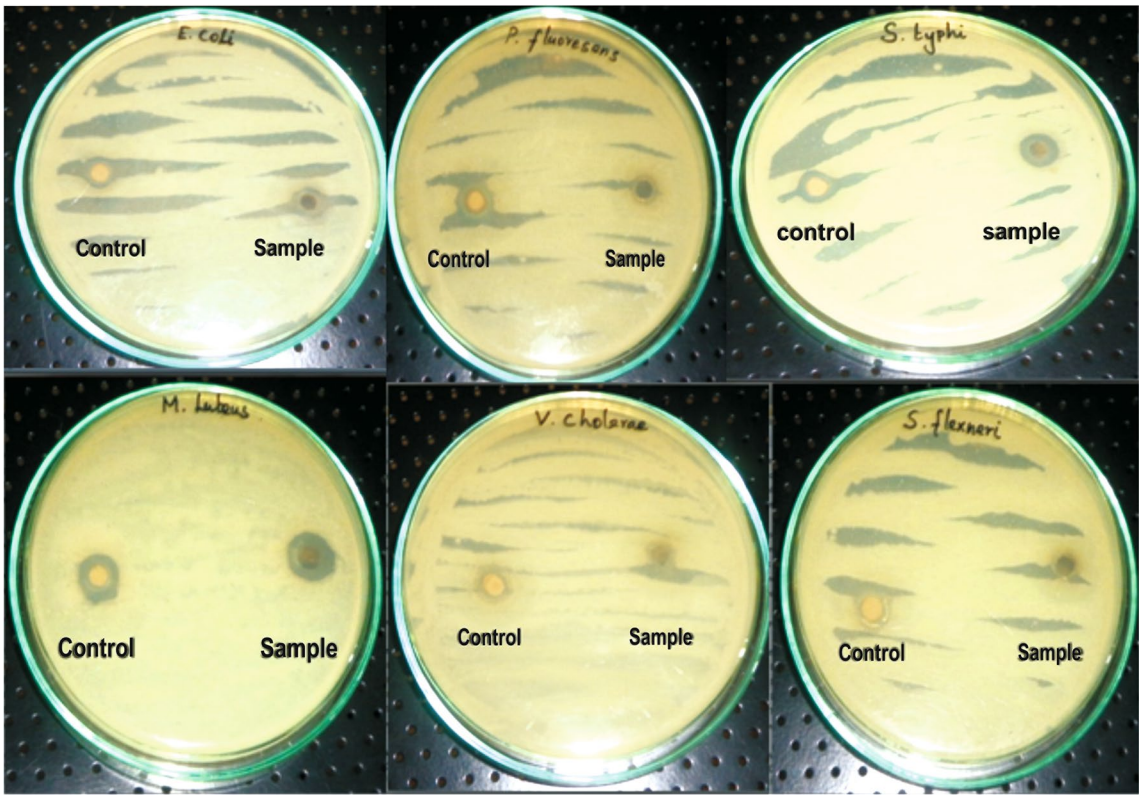

Fig. 7 Photographic image of an inhibition zone produced by CG against

4 Conclusion

In conclusion, CuO NPs were synthesized using the solution combustion method. The synthesized CuO NPs were characterized by optical, structural, functional, and morphological characterizations. The XRD analysis showed that the CuO NPs are having a monoclinic crystal structure. It is found that higher annealing temperature yields smaller CuO nanoparticles with an average crystallite size of ~ 45 nm for the combustion temperature of 300°C. The optical properties of confirms CuO nanoparticles formation, thereby exhibiting a lower band bap energy due to quantum containment. Further, the refractive index,

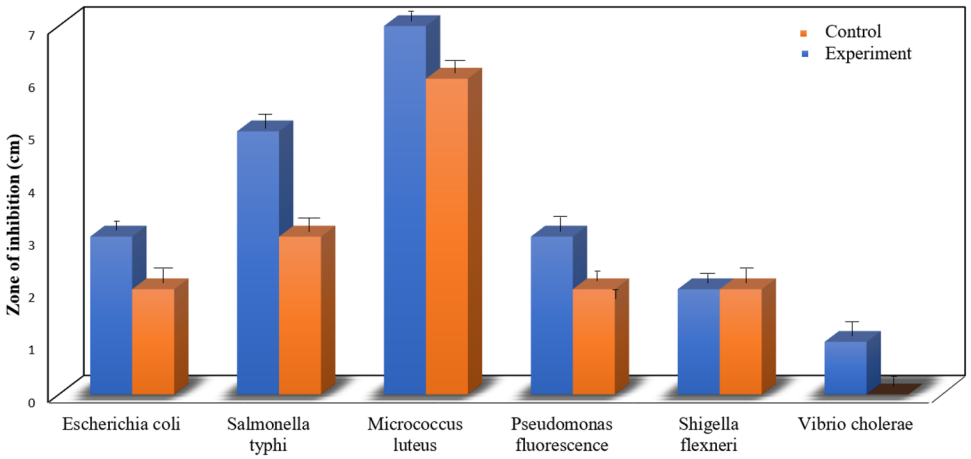

Fig. 8 The plot represents the antibacterial effect of CuO NPs on various microorganisms

optical dielectric constant and bulk modulus were investigated using the specific empirical model as a function of temperature. UV-using FTIR spectra, the different functional groups were studied. SEM confirms the spherical morphology of CuO NPs. EDAX analysis was confirmed by elements of CuO maximum composition. The CuO NPs have been studied for antibacterial activity. It was elucidated that due to their efficient antimicrobial efficacy, could represent efficient alternatives in the expansion of smart systems exploited for both recognition of pathogens and for the treatment of infections.

Acknowledgments The authors would like to acknowledge the financial support provided by Research University Grant Number (RU001-2018)NANOCAT, University of Malaya, Malaysia. One of the authors (Suresh Sagadevan) acknowledges the honor, namely the "Senior Research Fellow" at Nanotechnology and Catalysis Research Centre (NANOCAT), University of Malaya 50603 Kuala Lumpur, Malaysia. The author wishes to place on record his heartfelt thanks that are due to the authorities concerned.

Compliance with ethical standards

Conflict of interest The authors declare no conflict of interest.

References

1. Y. Yecheskel, I. Dror, B. Berkowitz, Catalytic degradation of brominated flame retardants by copper oxide nanoparticles. Chemosphere **93**, 172–177 (2013)
2. Q. Zhang, K. Zhang, D. Xu et al., CuO nanostructures: synthesis, characterization, growth mechanisms, fundamental properties, and applications. Prog. Mater Sci. **60**, 208–237 (2014)
3. P. Raksa, A. Gardchareon, T. Chairuangsri, P. Mangkorntong, N. Mangkorntong, S. Choopun, Ethanol sensing properties of CuO nanowires prepared by an oxidation reaction. Ceram. Int. **35**, 649–652 (2009)
4. A. Aslani, V. Oroojpour, CO gas sensing of CuO nanostructures, synthesized by an assisted solvothermal wet chemical route. Phys. B **406**, 144–149 (2011)
5. M. Yang, J. He, X. Hu, C. Yan, Z. Cheng, CuO nanostructures as quartz crystal microbalance sensing layers for detection of trace hydrogen cyanide gas. Environ. Sci. Technol. **45**, 6088–6094 (2011)
6. Y. Li, J. Liang, Z. Tao, J. Chen, CuO particles and plates: synthesis and gas-sensor application. Mater. Res. Bull. **43**, 2380–2385 (2008)
7. X. Wang, X. Xu, Thermal conductivity of nanoparticle-fluid mixture. J. Thermophys. Heat Transf. **13**, 474–480 (1999)
8. J. Singh, G. Kaur, M. Rawat, A brief review on synthesis and characterization of copper oxide nanoparticles and its applications. J. Bioelectron. Nanotechnol. **1**(1), 9 (2016)
9. M. Sahooli, S. Sabbaghi, R. Saboori, Synthesis and characterization of mono sized CuO nanoparticles. Mater. Lett. **81**, 169–172 (2012)
10. K.S. Khashan, G.M. Sulaiman, F.A. Abdulameer, Synthesis and Antibacterial Activity of CuO Nanoparticles Suspension Induced by Laser Ablation in Liquid. Arab. J. Sci. Eng. **41**, 301–310 (2016)
11. Vinod Vellora Thekkae Padil, Miroslav Černík, Green synthesis of copper oxide nanoparticles using gum karaya as a biotemplate and their antibacterial application. Int. J. Nanomed. **8**, 889–898 (2013)
12. P. Gong, H. Li, X. He et al., Preparation and antibacterial activity of Fe_3O_4@Ag nanoparticles". Nanotechnology **18**, 285604 (2007)
13. Y. Haldorai, J.-J. Shim, Multifunctional chitosan-copper oxide hybrid material: photocatalytic and antibacterial activities. Int. J. Photoenergy **2013**, 1–8 (2013)
14. P.S. Kumar, M. Selvakumar, S.G. Babu, S.K. Jaganathan, S. Karuthapandian, S. Chattopadhyay, Novel CuO/chitosan nanocomposite thin film: facile hand-picking recoverable, efficient and reusable heterogeneous photocatalyst. RSC Adv. **5**, 57493–57501 (2015)
15. A.M. El Sayed, S. El-Gamal, W.M. Morsi, G. Mohammed, Effect of PVA and copper oxide nanoparticles on the structural, optical, and electrical properties of carboxymethyl cellulose films. J. Mater. Sci. **50**(2015), 4717–4728 (2015)
16. M. Safari, M. Taran, Optimized synthesis, characterization, and antibacterial activity of an alginate–cupric oxide bio- nanocomposite. J. Appl. Polym. Sci. **135**, 45682 (2018)
17. S. Roy, J.W. Rhim, Melanin-mediated synthesis of copper oxide nanoparticles and preparation of functional agar/CuO NP nanocomposite films. J. Nanomat. (2019). https://doi.org/10.1155/2019/2840517
18. A. Paracchino, J.C. Brauer, J.-E. Moser, E. Thimsen, M. Graetzel, Synthesis and characterization of high-photoactivity

electrodeposited Cu_2O solar absorber by photoelectrochemistry and ultrafast spectroscopy. J. Phys. Chem. C **116**, 7341–7350 (2012)
19. T.D. Golden, M.G. Shumsky, Y. Zhou, R.A. Vander Werf, R.A. Van Leeuwen, J.A. Switzer, Electrochemical deposition of copper(I) oxide films. Chem. Mater. **8**, 2499–2504 (1996)
20. J.F. Pierson, A. Tobor-Keck, A. Billard, Cuprite, paramelaconite and tenorite films deposited by reactive magnetron sputtering. Appl. Surf. Sci. **210**, 359–367 (2003)
21. T. Maruyama, Copper oxide thin films prepared by chemical vapor deposition from copper dipivaloylmethanate. Sol. Energy Mater. Sol. Cells **56**, 85–92 (1998)
22. S. Sagadevan, K. Pal, Z.Z. Chowdhury, Fabrication of CuO nanoparticles for structural, optical and dielectric analysis using chemical precipitation method. J. Mater. Sci. Mater.Electron. **28**(17), 12591–12597 (2017)
23. S. Sagadevan, M. Priya, Electrical properties of copper oxide nanoparticles. J. Nano Res. **30**, 1–8 (2015)
24. K. Nakaoka, J. Ueyama, K. Ogura, Photoelectrochemical behavior of electrodeposited CuO and Cu_2O thin films on conducting substrates. J. Electrochem. Soc. **151**, C661–C665 (2004)
25. A.Y. Oral, E. Menşur, M.H. Aslan, E. Başaran, The preparation of copper (II) oxide thin films and the study of their microstructures and optical properties. Mater. chem. Phys. **83**(1), 140–144 (2004)
26. M. Izaki, M. Nagai, K. Maeda, F.B. Mohamad, K. Motomura, J. Sasano, T. Shinagawa, S. Watase, Electrodeposition of 1.4-eV-bandgap p-copper (II) oxide film with excellent photoactivity. J. Electrochem. Soc. **158**(9), D578–D584 (2011)
27. W. Shockley, H.J. Queisser, Detailed balance limit of efficiency of p-n junction solar cells. J. Appl. Phys. **32**, 510 (1961)
28. D. Gupta, S.R. Meher, N. Illyaskutty, Z.C. Alex, Facile synthesis of Cu_2O and CuO nanoparticles and study of their structural, optical and electronic properties. J. Alloy. Compd. **743**, 737–745 (2018)
29. N.M. Balzaretti, J.A.H. da Jornad, Pressure dependence of the refractive index of diamond, cubic silicon carbide and cubic boron nitride. Solid State Commun. **99**, 943–948 (1996)
30. N.M. Ravindra, S. Auluck, V.K. Srivastava, On the Penn gap in semiconductors. Phys. Status Solidi. (b) **93**, k155–K160 (1979)
31. P.J.L. Herve, L.K.J. Vandamme, Empirical temperature dependence of the refractive index of semiconductors. J. Appl. Phys. **77**, 5476–5477 (1995)
32. D.K. Ghosh, L.K. Samanta, G.C. Bhar, A simple model for evaluation of refractive indices of some binary and ternary mixed crystals. Infrared Phys. **24**, 43–47 (1984)
33. D.R. Penn, Wave-number-dependent dielectric function of semiconductors. Phys. Rev. **128**, 2093–2100 (1962)
34. J.A. Van Vechten, Quantum dielectric theory of electronegativity in covalent systems I. Electronic dielectric constant. Phys. Rev. **182**, 891–905 (1969)
35. G.A. Samara, Temperature and pressure dependences of the dielectric constants of semiconductors. Phys. Rev. B **27**, 3494–3505 (1983)
36. J.C. Phillips, *Bonds, and bands in semiconductors* (Academic Press, San Diego, 1973)
37. Y. Al-Douri, H. Abid, H. Aourag, Empirical formula relating the bulk modulus to the lattice constant in tetrahedral semiconductors. Mater. Chem. Phys. **87**, 14–17 (2004)
38. A. Barakat, M. Al-Noaimi, M. Suleiman, A.S. Aldwayyan, B. Hammouti, T.B. Hadda, S.F. Haddad, A. Boshaala, I. Warad, Effect of calcination temperature on Cu doped NiO nanoparticles prepared via wet-chemical method: structural, optical and morphological studies. Int. J. Mol. Sci. **14**, 23941–23954 (2013)
39. S. Sagadevan, J. Podder, Investigations on structural, optical, morphological and electrical properties of nickel oxide nanoparticles. Int. J. Nanoparticles **8**, 289–301 (2015)
40. Y. Liu, Y. Chu, M. Li, L. Lia, L. Dong, In situ synthesis and assembly of copper oxide nanocrystals on copper foil via a mild hydrothermal process. J. Mater. Chem. **16**, 192–198 (2006)
41. A. Kalam, A.G. Al-Sehemi, A.S. Al-Shihri, G. Du, T. Ahmad, Synthesis and characterization of NiO nanoparticles by thermal decomposition of nickel linoleate and their optical properties. Mater. Charact. **1**(68), 77–81 (2012)
42. R. Goyal, L.K. Macri, H.M. Kaplan, J. Kohn, Nanoparticles and nanofibers for topical drug delivery. J. Control. Release **240**(2016), 77–92 (2016)
43. I.M. El-Nahhal, S.M. Zourab, F.S. Kodeh, M. Selmane, I. Genois, F. Babonneau, Nanostructured copper oxide-cotton fibers: synthesis, characterization, and applications. Int. Nano Lett. **2**, 1–5 (2012)
44. M. Grigore, E. Biscu, A. Holban, M. Gestal, A. Grumezescu, Methods of synthesis, properties and biomedical applications of CuO nanoparticles. Pharmaceuticals **9**(4), 75 (2016)